UNIVERSITY POLITEHNICA OF BUCHAREST
Doctoral School - Faculty of Applied Chemistry and Materials Science
Department of Inorganic Chemistry, Physical Chemistry and Electrochemistry
Senate Decision No. 242 of 23.11.2017

DOCTORAL THESIS

Study of tin dioxide based ceramics for gas detection and corrosivity of fluids involved in fire extinguishing

SUMMARY

Author: Maj. Eng. Andrei-Dan BUSUIOC

Supervisor: Emeritus Prof. PhD. Eng. Teodor VIŞAN

BUCHAREST - 2017

Contents

INTRODUCTION

The field of ceramics for fuel gas sensors and the corrosivity problem in the case of the foam concentrates used for fire extinguishing are closely related to the engineering education of the author and to his activity for over nine years in emergency response units. The researches addressed in the thesis are of great importance and topicality, both for a wide range of industries involving the use of fuel gases, as well as for monitoring the environment and safety reasons for living organisms. Tin dioxide (SnO_2) is an oxide material that combines the electrical resistance sensitive to the nature and concentration of gases with a high chemical stability, properties necessary in the construction of gas sensors. In particular, SnO_2 based sensors are characterized by a high sensitivity, fast response and low production cost. Works on sensors related topics or centered on fire risk are frequently published in various scientific journals and magazines.

The objectives of the doctoral thesis include the preparation and characterization of a series of pure or doped SnO_2 structures, with possible applications in the fabrication of fuel gas sensors. The research begins with zerodimensional structures (powders), for which four different wet chemistry synthesis methods are tested, continues with sintering, to obtain ceramic masses, and ends with onedimensional structures in the form of electrospun fibers.

The investigation of the corrosivity of *6 % P Profoam 806* and *Foamtec P 6 %* foam concentrates used for fire extinguishing is the other main objective of the doctoral thesis, these concentrates being very aggressive in relation to the metallic materials they are in contact with. *Aluminium alloy*, from which different components of the hose reel couplings and foam nozzles are made, as well as *carbon steel*, which is the main construction material of the vessels for storing foam concentrates and related pipes, were selected for research. There is a lack of data in the literature on these proposed systems, which results in the absolute novelty and originality of the conducted studies.

The doctoral thesis consists of nine chapters, two of which are literature studies, five chapters present the original contributions, one chapter is devoted to the conclusions and another chapter displays the bibliography.

The part of **Literature Data** begins with **Chapter 1**, which describes the results published in the specialty literature on ceramic materials for gas sensors. Firstly, there is a broad discussion on gas sensors (classifications, history, working principle), which is then particularized to SnO_2 based sensors. The chapter ends with the presentation of some synthesis methods for SnO_2 structures with different dimensionalities.

Chapter 2 is devoted to the issue of fire extinguishing foams and their aggressiveness on metallic equipments of the fire trucks employed by firefighters. There are described the foam classes, the history of their development and the implications on environmental pollution, providing then examples of corrosion cases in situations where fire extinguishers, sprinklers, couplings, nozzles, flame retardants are used. The chapters from the part of **Literature Data** are illustrated with 40 Figures and 8 Tables, quoting 195 bibliographic references.

The part of **Own Contributions** begins with **Chapter 3**, which contains original experiments on the preparation and characterization of SnO_2 powders, as a first step for the development of applications in the field of gas sensors. There is comparatively studied the solution synthesis by precipitation, sol-gel, Pechini and hydrothermal methods. Powders characterization was performed by thermal analysis, X-ray (XRD) and electron diffraction, scanning (SEM) and transmission (TEM) electron microscopy and laser granulometry. A subchapter is dedicated to the synthesis and characterization of SnO_2 powders doped with La^{3+} or V^{5+}, which may have improved gas detection performance compared to pure SnO_2; in this case, UV-Vis spectroscopy is added as investigation method.

Chapter 4 continues the research with the obtaining and characterization of some SnO_2 based ceramics, pure and doped with La^{3+} or V^{5+}. The precursor powders were obtained by the precipitation method from solution. This was followed by ceramics thermal treatment and density determinations, as well as the investigation of the compositional, structural and morphological modifications generated by the sintering process, using XRD and SEM coupled with energy dispersive X ray spectroscopy (EDX). Also, the influence of dopant and thermal history on the sensitivity to methane and isopropyl alcohol vapors was highlighted.

Chapter 5 presents the synthesis of onedimensional structures in the form of SnO_2 fibers electrospun from a solution containing polyvinylpyrrolidone as sacrificial polymer. The calcination parameters (heating rate, maximum temperature and period of time at maximum temperature) of the precursor fibers were varied and their effect on the crystalline structure, morphology and composition was investigated by XRD and SEM coupled with EDX. Based on the UV-Vis spectra of calcined fibers, the bandgap energy values were estimated.

Chapter 6 includes data on the corrosivity study of *6 % P Profoam 806* and *Foamtec P 6 %* foam concentrates by gravimetric measurements of the corrosion rate at long term immersion of metallic materials (aluminium alloy and carbon steel). The corrosion rates, expressed as gravimetric index and penetration index, were determined from the weight loss. The morphological and compositional characterization of the surface was performed by SEM coupled with EDX, before and after the corrosion process, observing the occurrence of corrosion products, as well as the chemical concentrations evolution for the alloying elements and newly formed compounds.

Chapter 7 adds new information to the corrosion investigation of selected materials using two electrochemical methods: potentiodynamic polarization curves (Tafel) and electrochemical impedance spectroscopy. The determination of the corrosion potential and corrosion current density was achieved by cyclic polarization under potentiodynamic conditions. Complementary information was obtained from the electrochemical impedance spectra at open circuit potential and a number of increasingly positive potentials that simulate the advancement of metal anodic dissolution. For both metallic materials, the experimental impedance data were modeled with a Randles equivalent electrical circuit. The part of **Own Contributions** is illustrated with 74 Figures and 24 Tables.

The thesis ends with conclusions and a bibliography containing 321 bibliographic references.

The original results of the doctoral thesis were partially disseminated in four papers published in specialized journals (three ISI quoted and one ISI indexed), as well as two papers presented by the author at international scientific conferences.

The present summary contains in a concise form the content of all chapters, refering to the literature survey and original contributions of the author. The content and numbering of figures, tables, and bibliographic references correspond to those in the thesis.

Keywords: SnO_2; Semiconductors; Ceramics; Fibers; Wet chemistry methods; Electrospinning; Bandgap; Corrosion; Fire extinguishing foam concentrates; Aluminium alloy; Carbon steel; Electrochemical methods; Randles circuit.

PART I. LITERATURE DATA

Chapter 1
Ceramic materials for the field of gas sensors

1.1. General concepts of gas sensors
1.1.1. Classifications and fields of use for gas sensors

In a broad sense, a sensor is a device that reacts to any change that occurs in processes characterized by parameters such as: temperature, pressure, humidity, motion, etc. This change affects the physical, chemical or electromagnetic properties of the sensor, which will then process the input signal and convert it into an output signal. As for the quantitative aspect, the signal produced by the sensor is directly proportional to the measured parameter.

In order to evaluate the performance of a gas sensor, a wide range of indicators should be considered, as follows: **sensitivity**, **selectivity**, **response time**, **reversibility**, **adsorption capacity**, **energy consumption**, **manufacturing cost**. [4]

In terms of presentation form, gas sensors can be divided into **portable devices** and **fixed devices**. Depending on the gas detection technology, sensors are classified as: **catalytic combustion sensors**, **electrochemical sensors**, **semiconductor metal oxide based sensors**, **infrared sensors**, **photoacoustic sensors**, **ultrasonic sensors**. [8]

One of the most important categories of sensors uses semiconductor metal oxides as active materials. The capability to detect gases is closely correlated with their electronic structure, the latter causing the distribution of metal oxides into two large categories:
- transition metal oxides (NiO, Mn_2O_3, TiO_2, V_2O_5, WO_3 etc.);
- non- transition metal oxides, which in turn can be:
    - pre-transition metal oxides (MgO, Al_2O_3 etc.);
    - post-transition metal oxides (ZnO, SnO_2 etc.). [9]

1.1.2. History of gas sensors development

From the primitive variants of gas sensors, it has now come to devices with autonomy of operation for long periods of time due to the use of accumulators, as well as to modern detectors capable of detecting more gases simultaneously. [11]

As far as the modern history of gas sensors is concerned, this is closely related to the evolution of the industry producing such measuring and control devices. One of the world largest companies in the field is Figaro (Japan). The engineer N. Taguchi founded the company in 1962, being the first person in the world who developed a semiconductor device for detecting low concentrations of fuel and reducing gases, integrated into a simple electric circuit (1968), known as Taguchi Gas Sensor. This uses tin dioxide (SnO_2) as active material. In the 90s, the company implemented innovative manufacturing techniques for semiconductor gas sensors, of which the thick film printing technology can be mentioned. Subsequently, the attention was focused on the manufacturing of electrochemical sensors. The current concerns include the expanding of gas

chromatographic technology, creating a more comfortable environment by using gas sensors and measuring the gases and odors produced by the human body in healthcare applications. [12]

1.1.3. Working principle of gas sensors

The chemical detection can be considered as a two step process: **reception function** (chemicals identification) and **transmission function** (translation of the chemical signal into an output signal). While the former is made by the surface of each grain, the entire microstructure of the active material is involved in the second.

The exact mechanism of gas detection using metallic oxides is still controversial, but electron capture by oxygen molecules and the bandgap upwards bending, induced by the formation of electrically charged oxygen species, are responsible for changing the conductivity in the sense of reducing it. The reaction of oxygen species with the reducing gases or the adsorption and competitive exchange of adsorbed oxygen by other molecules results in the decrease and even the bandgap downwards bending, leading to an increase in conductivity. [16]

Thus, the working principle of gas sensors is based on the detection of the conductivity changes suffered by the active material. Since gas adsorption is related to the material surface, polycrystalline structures, even nanocrystalline, are preferred. [17]

The gas detection capability is influenced by a number of factors, among which the most important are: **chemical composition**, **microstructure**, **environment humidity and operating temperature**.

1.2. Tin dioxide (SnO_2) based gas sensors
1.2.1. SnO_2 structure

Tin dioxide (SnO_2), also known as stannic oxide, consists of O and Sn, the latter having +4 oxidation state. SnO_2 has a rutile structure (tetragonal crystallization system), wherein each Sn atom is surrounded by six O atoms in an octahedral configuration and each O atom is surrounded by three Sn atoms in a planar layout. [26]

SnO_2 is a *n*-type semiconductor, with a wide bandgap of approximately 3.6 eV, being one of the most used semiconductors due to its transparency, chemical stability and mechanical properties. Pure SnO_2 conductivity is provided by oxygen vacations that act as electron donors. [17]

1.2.2. Improvement of SnO_2 properties by doping

The addition of secondary components in the composition of semiconductor metal oxide based sensors is a means of optimizing the detection systems properties. These additions may act as additives or dopants. In the case of dopants, the action can be expressed at several levels: generating active sites for redox processes, promoting of charge carriers to improve the electrical conductivity or controlling the crystals size and inhibiting the growth of constituent grains to enhance the sensitivity. Depending on valence, dopants may be: **donors** or **acceptors**. [31]

Some examples of materials used to adjust SnO_2 properties were approached, starting from simple systems (doping cations) and going to complex systems (codoping, composites, structures with controlled morphology): **noble metals**, **Al and Sb**, **transition metals**, **rare earths**.

1.2.3. Synthesis methods for SnO_2

The following techniques were briefly described: **precipitation**, **sol-gel**, **combustion**, **electrospinning**, **pulsed laser deposition**.

1.2.4. SnO$_2$ based devices

Figaro Engineering Inc. company (Japan) is the world leader in the gas sensors industry. Most sensors are based on SnO$_2$, whose resistivity in the presence of fresh air is very high, decreasing considerably after the reducing chemical reaction of fuel gases, volatile organic compounds and many others. Regarding the fields of use, the most important are those of safety, health, control systems and measuring instruments. [12]

All marketed devices have low power consumption, high sensitivity, long life and low cost and use a simple electrical circuit.

Several typical devices are listed below:

● **TGS2610 - fuel gas sensor (GPL)**;
● **TGS2611 - methane sensor (methane)**;
● **TGS5042 - carbon monoxide sensor (CO)**;
● **TGS823 - organic solvent vapor (alcohol, solvent vapor) sensor**;
● **TGS2603 - air contaminants sensor (trimethilamine, methilmercaptan etc.)**.

[12]

Chapter 2
Fire extinguishing foams and their aggressiveness on metallic equipments used by firefighters

2.1. General concepts of fire extinguishing foams
2.1.1. Classifications and fields of use for foams

The foam is used to extinguish fuel liquids lighter than water, stored in tanks or leaked to the ground. It cannot be used where the presence of water is prohibited.

From the point of view of production, Romanian standards classify the foams in two categories: **chemical foam** and **mechanical foam** (*heavy* or *light*). A more recent variety of mechanical foam with special properties is **light water**.

The international classification of foams is correlated with the fire classes (A - F). **Class A foams** and **class B foams** should be mentioned, the latter being either *synthetic foams* (based on surfactants prepared by chemical synthesis) or *natural foams* (contain natural proteins as foaming agents, resulted from a degradation process with mineral acids, neutralization and stabilization with appropriate chemicals).

2.1.2. History of fire extinguishing foams development

A. Loran is considered to be the inventor of the fire foam, in 1902. In 1904, he patented his invention and developed the first foam extinguisher (called *chemical foam*), consisting of a mixture of two powders and water and produced in a foam generator. In the 40s, P.L. Julian developed a new type of foam, the protein foam (called *Aerofoam*), which greatly improved the fire extinguishing capability and reduced the production costs. In the early 50s, H. Eisner developed the high expansion foams, used for extended locations. In the 60s, flouroprotein foams were applied. In the mid 60s, the American marine developed the aqueous film forming foam [120]. In the early 70s, it was developed a product that solved many serious extinguishing problems, applicable for fires involving alcohols and polar solvents.

In 1993, the wetting agents (called *wet water*) appeared, with superior cooling properties, which were efficient for classes A, B and D fires, as well as for threedimensional and under pressure fires, involving both hydrocarbon based fuels and polar solvents. The foam with wetting agent was first marketed under the name of *Pyrocool*, but it was later found to have major negative effects on water sources, but also environmental implications. Significant progress in the search for substitutes was made in 2010, materialized by the development of fluorine free foams, the most performing foam in this category being marketed under the name *BluFoam*.

The legislation from many countries, including the European Union [123], prohibits certain components incorporated in a series of foam concentrates. The studies showed that perfluorooctanesulfonic acid (PFOS) is a persistent, bioaccumulative and toxic pollutant for the aquatic and terrestrial environment [124-127]. Therefore, after 2004, its replacement with new fluorinated surfactants was requested.

2.1.3. Commercial fire extinguishing foams

The aqueous film forming foam concentrates (AFFF) have the following composition: synthetic foaming agents, organic solvents, surfactants with fluoro groups, low concentrations of inorganic salts and foam stabilizers.

Chemguard concentrates [147] combines the technologies for fluorosurfactants and hydrocarbon surfactants for the preparation of class B foams of type 3 or 6 %.

Solberg concentrates [148] are designed for extinguishing fires from class A and B, generating several types of foams: *FIRE-BRAKE* for class A, *RE-HEALING*, *ARCTIC* and *SOLBERG HIGH-EXPANSION* for class B.

LCF concentrates (Langchao Fire Technology) [149] for fluoroprotein foam of type *FP 3 %* and *FP 6 %* are applicable to class B fires; they contain the hydrolyzed fluoroprotein component and fluorosurfactant.

Ansul concentrates [150] contain amounts of synthetic fluorosurfactant, but in much lower concentration.

Angus Fire concentrates [151] are especially recommended for fires with liquid hydrocarbons, the produced foam being very compact and dense.

Capstone and Forafac concentrates [152] replace perfluorooctanesulfonic acid (PFOS) and are manufactured under different codes: *1157, 1157, 1183* etc.

Profoam concentrates [153, 154] are available in different assortments: *Profoam 806*, *Centrifoam 906*, *Fluorofoam 906*, *Filmfoam 836* and *Filmfoam 916*.

2.2. Corrosion of materials for fire extinguishing equipments
2.2.1. Corrosion mechanism and forms of corrosion

The foam concentrates for fire extinguishing are stored in the steel vessels of the trucks used to effectively extinguish the fuel fires. However, in the case of carbon steels, the foam is corrosive and may drill the tank walls, the resulting holes incurring costs for welding them. As a result, in many cases, aluminium alloys replace steels in the equipments employed by firefighters [172-177].

The publication from reference [183] describes and exemplifies different types of corrosion: uniform corrosion, galvanic corrosion, pitting corrosion, crevice corrosion, selective dissolution corrosion, corrosion - erosion, stress cracking, intergranular corrosion.

2.2.2. Effects of corrosion on fire extinguishing installations

Corrosion in ordinary fire extinguishers. There have been cases where the corrosion located at the bottom of the fire extinguisher was sufficiently advanced that it cracked at the moment of activation and the broken parts spread, sometimes injuring the people in the neighborhood [178].

Corrosion in various types of sprinkler systems. Internal corrosion in a spraying installation may cause partial or complete blocking, thus reducing the water flowability. It can also lead to pipes and fittings deterioration. In most cases, the system corrosion is caused by the presence of water and air inside. The decreasing of system corrosion can be done by filling with compressed nitrogen instead of air. Considering the welded carbon steel pipes [170, 181], the corrosion is preferential to the weld seam. In all installations, microbiological corrosion also occurs, because microorganisms are ubiquitous.

Corrosion in installations with external foam formation. In the practice of extinguishing fires in our country, water and foam are delivered through a hydraulic chain that starts with the centrifugal pumps, continues with the hose reels and ends with the nozzles [168] The hoses are connected to pumps or hydrants via couplings. Romanian firefighters employ the so called Storz type couplings made of AlSi5Cu1Mg alloy cast

under pressure. Recently, new nozzles (spray type) with superior characteristics than standard were developed [188].

Corrosion studies in flame retardants. A special category of liquids involved in fire prevention is represented by the flame retardants. These can cause excessive corrosion on storage tanks, foam preparation vessels, as well as helicopters or planes that scatter them over large areas.

PART II. OWN CONTRIBUTIONS

Chapter 3
SnO₂ powders for gas sensors

3.1. Introduction

SnO_2 is rarely used in its pure form, generally being associated with impurities or dopants. In gas detection, these additives increase the sensitivity and selectivity for certain gases [29]. Moreover, this oxide was obtained in various morphological forms, from massive body [211] to thin films [36, 212], from onedimensional structures [60, 213] to zerodimensional structures [75, 214, 215]. Going to synthesis, the wet chemistry methods have some advantages over the conventional ones, providing good control of stoichiometry, purity, homogeneity and morphology, while significantly reducing the processing temperature [202, 203, 216]. The precipitation [217, 218], sol-gel [219], hydrothermal [220], combustion [75] and pyrolysis [221] methods can be mentioned from this category.

3.2. SnO₂ powders prepared by wet chemistry methods
3.2.1. Experimental part

The precipitation procedure was carried out under basic conditions, which led to the precipitation of Sn^{2+} ions from the solution obtained by dissolving the required amount of $SnCl_2 \cdot 2H_2O$ in a minimum volume of distilled water. For the sol-gel method, the white precipitate was dissolved in glacial acetic acid and then ethylene glycol was added to the solution to provide the formation of tin complexes. Finally, the Pechini method was carried out starting from a solution of $SnCl_2 \cdot 2H_2O$ in ethylene glycol, to which a quantity of citric acid was added; a resin precursor was obtained by esterification, which was subsequently burned. Turning to the hydrothermal technique, it began with the preparation of a $SnCl_4 \cdot 5H_2O$ solution in distilled water, which was then subjected to the autoclaving process, either as such or with different additions. [224,225]

3.2.2. Results and discussion

The thermal analyses performed on the intermediate materials obtained by the three approached wet chemistry methods allowed the calcination temperatures setting: 400 °C for the precipitation method, 500 °C for the sol-gel method and 800 °C for the Pechini method.

The calcined samples contain SnO_2 with tetragonal symmetry, except for the powders prepared by the Pechini technique, where a small fraction of secondary phase is present.

In the case of the precipitation method, the calcined powder consists of quasispherical or polyhedral particles with dimensions from several nm to tens of nm, but also some particles with prismatic shape. The gel derived powder exhibits particles in a wide dimensional range: fine spherical particles with dimensions less than 10 nm, medium

quasispherical or polyhedral particles with dimensions less than 1 μm and large irregular μm particles. In the third case, the particles from the calcined powder are more rounded and uniform in size, with an average diameter of 80 nm, while the laced and fluffy minor phase may be associated with the secondary phase.

Figure 3.4 presents the specific curves recorded with the help of a laser granulometer, using water as dispersion medium. The fine granulometric fraction, with dimensions below 1 μm, is highlighted for both precipitation and sol-gel methods, while the bands located at larger particle sizes can be attributed to the presence of aggregates that could not be separated by ultrasonication. Going to the Pechini technique, most of the particles appear to be placed at about 100 μm; this means that the individual particles are strongly gathered in the form of compact agglomerations, as a consequence of the high calcination temperature.
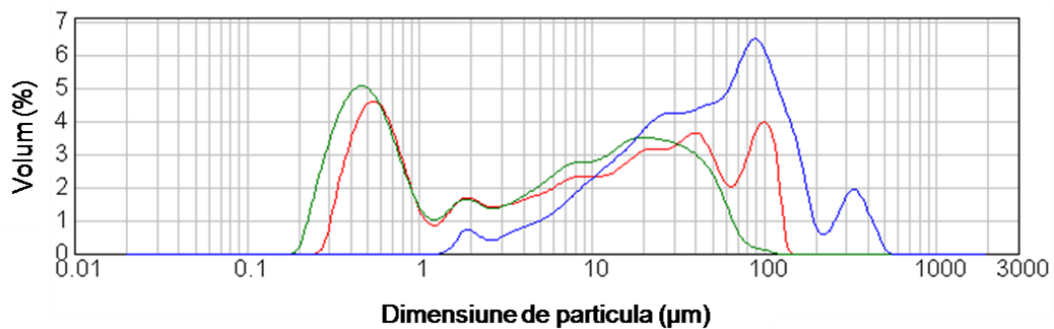
Figure 3.4. Particle size distribution curves for SnO_2 powders
synthesized by different wet chemistry methods
(red - precipitation, green - sol-gel, blue - Pechini).

Regarding the hydrothermal method, the powders contain the same crystalline phase, but with small crystals. For a more detailed characterization of the powders previously discussed, the TEM technique associated with electron diffraction (Figure 3.7) was used. The TEM images reveal the existence of large agglomerations, whereas the HRTEM images highlight crystals with diameter of few nm. Also, the electron diffraction patterns are specific for a polycrystalline material.
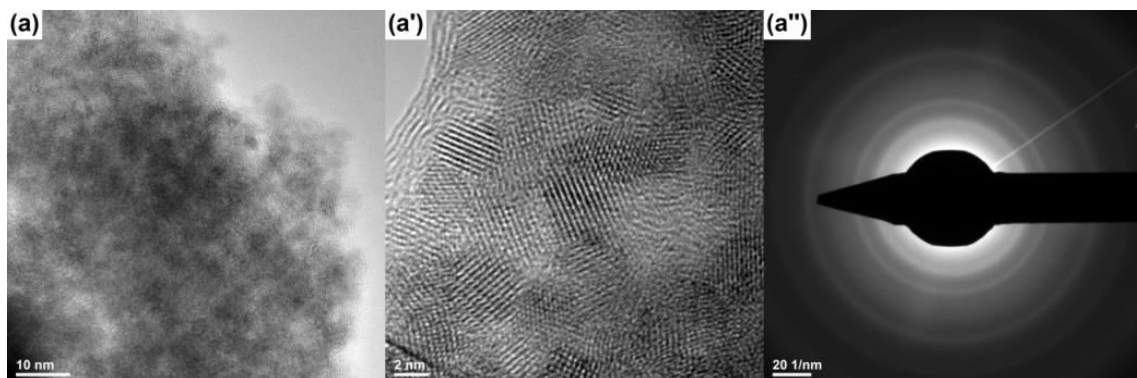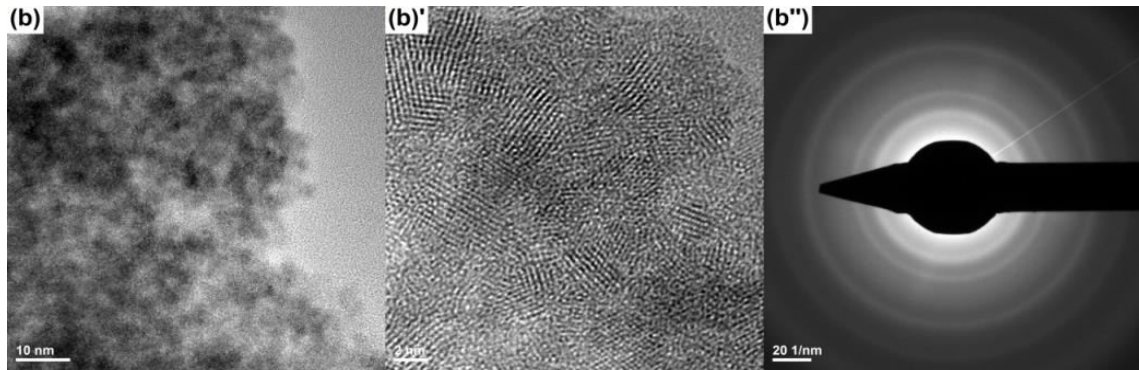
Figure 3.7. TEM and HRTEM images and electron diffraction patterns for SnO_2 powders synthesized by the hydrothermal method: ht3 (a, a' and a'') and ht4 (b, b' and b'').

3.3. SnO_2 powders doped with La^{3+} or V^{5+}
3.3.1. Experimental part

SnO_2 powders were prepared by the precipitation method. $SnCl_2 \cdot 2H_2O$ was weighted and dissolved in a minimum volume of distilled water. To this clear solution it was added the dopant solution obtained by solubilizing La_2O_3 or NH_4VO_3 in hydrochloric acid so as to provide a dopant concentration of 0.5, 1.0 or 2.0 wt%. After homogenization, the *p*H was changed to basic values, which led to the precipitation of Sn^{2+} ions [227]. The resulting suspension was filtered and the white precipitate was collected, washed, dried and calcined. [226]

3.3.2. Results and discussion

The thermal analysis validated a calcination temperature of 400 °C. The X-ray diffraction patterns for the calcined powders (Figure 3.9) demonstrate the formation of SnO_2 with tetragonal structure. Only for the high dopant concentrations appear some supplementary peaks, which can be explained on the basis of a high concentration of dopant that could not be fully integrated into the crystalline network.
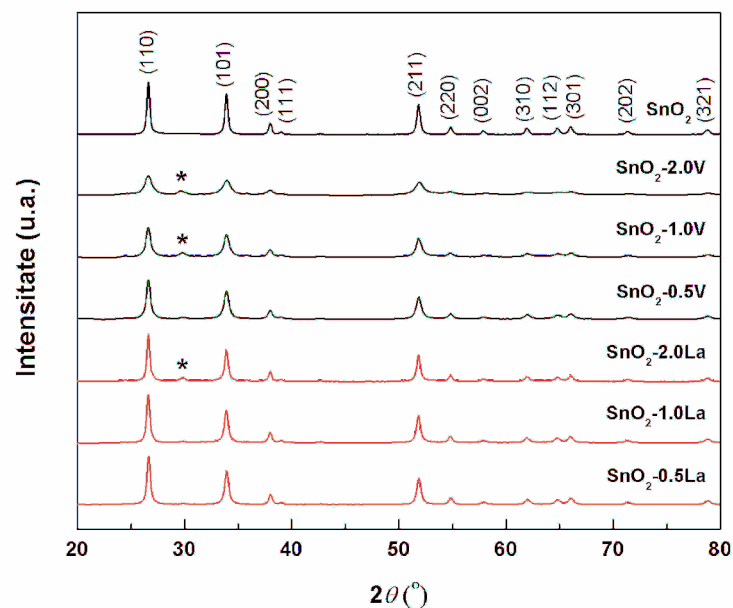
Figure 3.9. X ray diffraction patterns for the calcined SnO_2 powders. * indicates secondary phases.

The powders consist of aggregates of different sizes, typical of the precipitation method. The individual particles are quasispherical or polyhedral, with dimensions from several nm to tens of nm. In terms of dopant influence on the morphological properties of SnO_2 powders, lanthanum results in larger and more rough particles, while vanadium does not affect the particles shape and size.

Starting from the UV-Vis spectra of the calcined powders and using Kubelka-Munk graphical representations, the bandgap values were extracted, as shown in Table 3.2. The doped powders show a left shift of the bandgap, namely a reduction of the bandgap as a consequence of dopant penetration into the crystalline network. It is also obvious that vanadium has a stronger influence, in other words, a significant decrease of the bandgap even for a low dopant concentration.

Table 3.2. Average crystallite size and bandgap values for the calcined SnO_2 powders.

No.	Dopant	Concentration *(wt%)*	Average crystallite size *(nm)*	Bandgap *(eV)*
1	-	-	53	3.55
2	La^{3+}	0.5	46	3.10
3		1.0	47	3.02
4		2.0	54	2.86
5	V^{5+}	0.5	36	2.98
6		1.0	32	2.82
7		2.0	21	2.78

Chapter 4
SnO$_2$ based ceramics for gas sensors

4.1. Introduction

Many fabrication methods were used to produce semiconductor metal oxide based gas sensors, but the conventional approaches remain the most embraced at industrial level, even if they involve high processing temperatures [248]. However, hybrid or unconventional techniques gained ground lately, showing their huge potential for optimizing the material properties [245, 246, 249].

4.2. Experimental part

Pure and doped SnO$_2$ based ceramics were obtained from powders prepared by the precipitation method. La^{3+} and V^{5+} were used as dopants, the proportions selected for the corresponding oxides being 0.5, 1.0 or 2.0 wt%. The calcined powders were uniaxially pressed into disks and then sintered at 1300, 1400 or 1500 °C. [255]

4.3. Results and discussion

Of the ceramic properties, the most representative parameter is the relative density. The presence of La^{3+} in any proportion causes an accentuated decrease of the relative density. In the case of V^{5+}, the trend is changed, namely the decrease of the relative density, generated by a small amount of dopant, is followed by a pronounced increase for larger quantities of foreign cations. For both dopants, a minimum of property is recorded for the concentration of 0.5 wt%.

All specimens consist of SnO$_2$ with tetragonal structure. In addition, for the higher sintering temperatures and especially for the higher content of La^{3+}, a secondary phase (La$_2$Sn$_2$O$_7$) can be observed. Comparing the current results with those reported for doped SnO$_2$ powders [226], it can be stated that the thermal treatment determined the total incorporation of V^{5+} content into the crystalline network, while the effect was completely opposite for La^{3+}, generating a separate lanthanum rich phase.

The evolution of the nanometric powders synthesized by the precipitation method is towards densified bodies made up of polyhedral granules with rounded edges and corners and dimensions up to more than 10 μm. Generally, the increase of the processing temperature favors the granular growth and porosity reduction. Furthermore, the secondary phase is found in the form of round and small particles dispersed on the surface of larger SnO$_2$ grains. The increase of La^{3+} concentration is accompanied by the emergence of more secondary phase, which forms a laced architecture as a result of grains connection on a large scale. V^{5+} mainly affects the grain size of SnO$_2$ based ceramics, doped with 0.5 or 1.0 wt%, leading to even 10 times larger grains, while in the case of 2.0 wt% content, the shape is also changed into more elongated grains.

The gas sensitivity of the obtained pure and doped materials was evaluated for two different media: methane and isopropyl alcohol vapors. To eliminate the influence of bodies size and shape, the electrical resistance was recorded both in the absence and presence of contaminants, after which the sensitivity was calculated. La^{3+} doped ceramics do not appear to be very sensitive to methane (Figure 4.7a), but in the case of isopropyl

alcohol vapors, a maximum sensitivity is reached for the concentration of 1.0 wt% (Figure 4.7b).
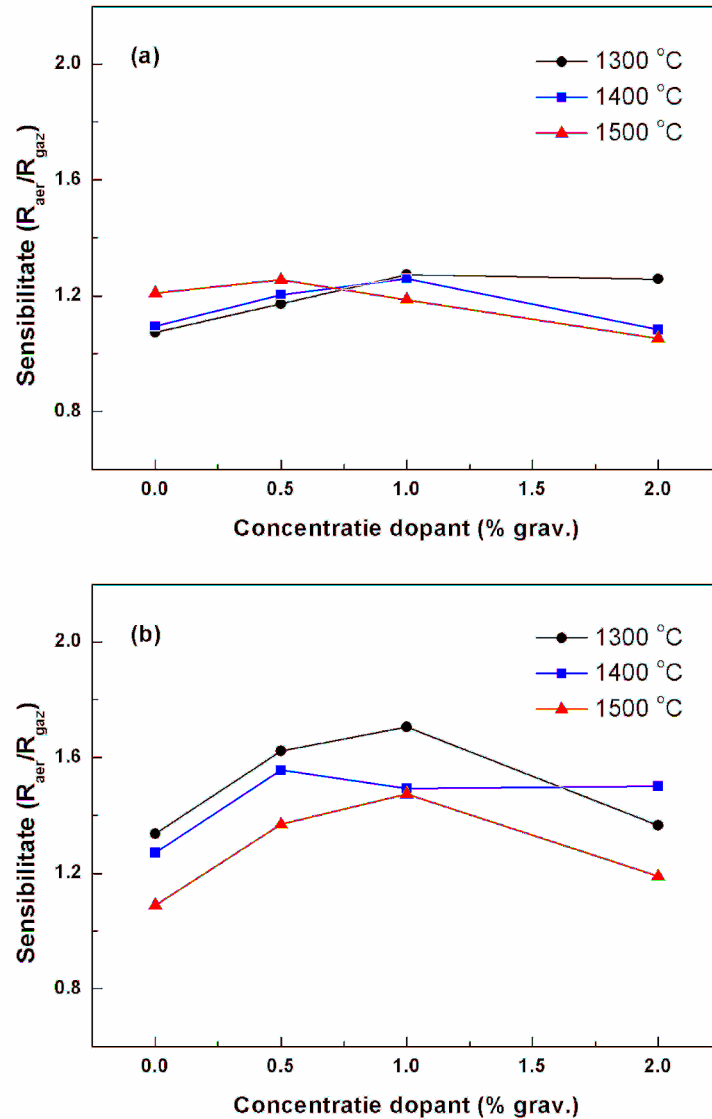
Figure 4.7. Variation of the sensitivity to methane (a) and isopropyl alcohol vapors (b) of SnO$_2$ based ceramics as a function of the sintering temperature and La^{3+} dopant quantity.

The use of V^{5+} as a dopant for SnO$_2$ increases its sensitivity to methane, the best behavior being also observed for the proportion of 1.0 wt% (Figure 4.8a), compared to isopropyl alcohol vapor exposure, when 0.5 wt% doping provides optimal results (Figure 4.8b).

By analyzing the implications of the sintering temperature for all discussed cases, it is obvious that a higher value for this parameter is not recommended because it naturally involves a better densification, phenomenon that has negative effects on the sensor active surface.

From the previous results, it is worth noting that by doping it is possible to adjust not only the sensitivity, but also the selectivity of SnO$_2$ based sensors.
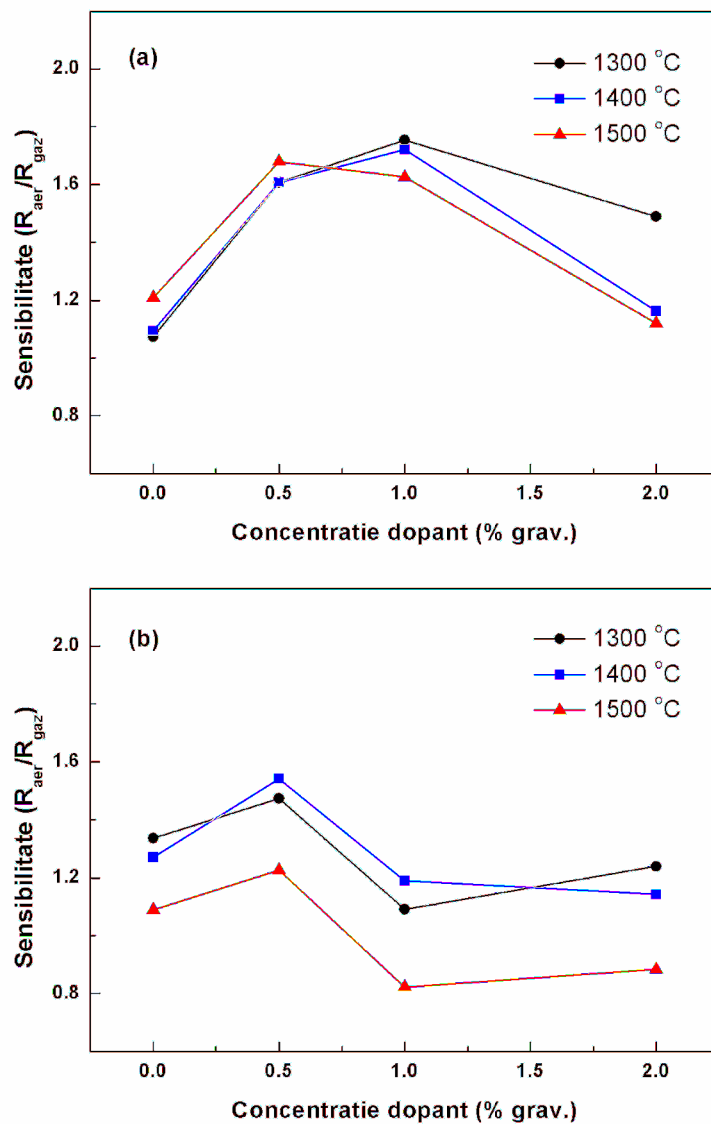
Figure 4.8. Variation of the sensitivity to methane (a) and isopropyl alcohol vapors c (b) of SnO$_2$ based ceramics as a function of the sintering temperature and V^{5+} dopant quantity.

Chapter 5
Electrospun SnO₂ fibers: Morphological and optical properties

5.1. Introduction

The synthesis of SnO_2 based onedimensional materials was accomplished especially by the electrospinning technique [78, 262-264, 267-269, 271, 272, 278], which is a simple, versatile and environmentally friendly approach for the fabrication of polymeric or inorganic fibers [279]. Several carrier polymers were used to prepare SnO_2 structures, such as: polyvinylpyrrolidone [263, 265, 267, 269, 271, 272, 278], polyvinyl alcohol [264], polyacrylonitrile [280], polyvinyl acetate [281].

5.2. Experimental part

SnO_2 fibers were prepared by the electrospinning technique, using $SnCl_2 \cdot 2H_2O$, polyvinylpyrrolidone and N,N-dimethylformamide to prepare the precursor solution. After optimizing the electrospinning conditions, the following values were chosen: feeding rate 0.5 mL/h, applied voltage 15 kV and working distance 15 cm. The next step was the calcination of the electrospun samples to determine the organic components removal, as well as SnO_2 crystals nucleation and growth. The thermal treatment parameters were: heating rate 1 or 10 °C/min, maximum temperature 500, 700 or 900 °C and 2 hours period of time at the mentioned temperatures. [282]

5.3. Results and discussion

The thermal analysis performed on the precursor fibers (Figure 5.1) indicated that the minimum temperature at which the electrospun fibers must be calcined is 500 °C.
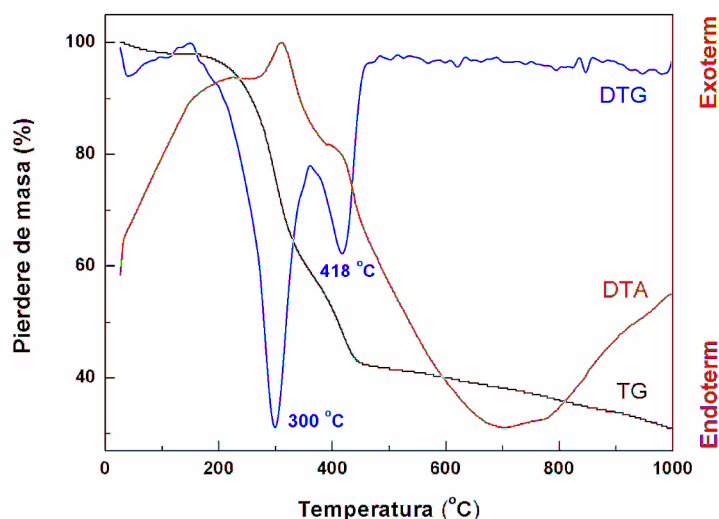
Figura 5.1. Thermal analysis on the electrospun fibers: thermogravimetric analysis (TG), the derivative of the themogravimetric analysis with respect to time (DTA) and differential thermal analysis (DTA).

The onedimensional precursor structures are randomly deposited on the substrate, in the form of nonwoven mesh, and have a uniform thickness over the entire length, the mean thickness being estimated at about 400 nm, while the length may reach even hundreds of nm. The thermal process allowed the obtaining of SnO_2 with rutile crystalline structure as single phase.

A reduction of approximately 25 % of the diameter was observed for all samples, explained on the basis of organic part combustion, while the dimensional uniformity was maintained. Nucleation, growth and densification processes of the oxide phase are governed by different laws, depending on the calcination temperature and heating rate. For 1 °C/min (Figure 5.4), the fibers are made up of quasispherical grains, whose average size increases with temperature increasing from less than 20 nm (500 °C) to about 40 nm (700 °C) and 50 nm (900 °C). Furthermore, an increase in porosity can be seen.
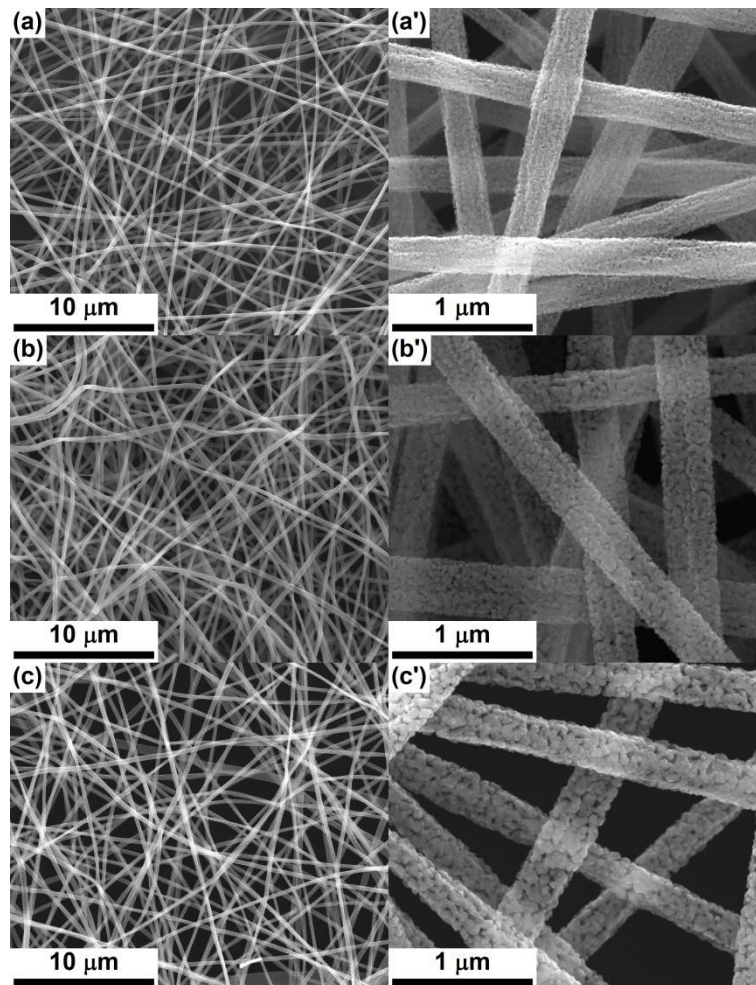
Figura 5.4. SEM images of SnO_2 fibers calcined at: 500 °C (a and a'), 700 °C (b and b') and 900 °C (c and c'), for 1 °C/min heating rate.

The acceleration of heating (10 °C/min) causes important changes in the morphology and a pronounced fragility of SnO_2 fibers, especially for the calcination temperature of 500 °C. The increase of the temperature to 700 or 900 °C has a positive effect on the fiber resistance structure, so that the cases of material breakage are fewer or even nonexistent. A higher heating rate inhibits the grain growth, the average size being below 20 nm for 500 °C, around 30 nm for 700 °C and 40 nm for 900 °C.

Starting from the UV-Vis spectra of the calcined fibers and using the Kubelka-Munk graphical representations, the banedgap values were extracted and the results are shown in Figure 5.8. The bandgap width increases with the calcination temperature increasing due to an expected improvement in the crystalline network ordering, together with a reduction in the defect concentration. Moreover, a low heating rate results in smaller bandgap values, in correlation with material evolution from structural and ceramic point of view. Taking into account the tendency of the average crystallite size and average grain size with the processing conditions, the shift of the bandgap could be attributed to a size effect [205].
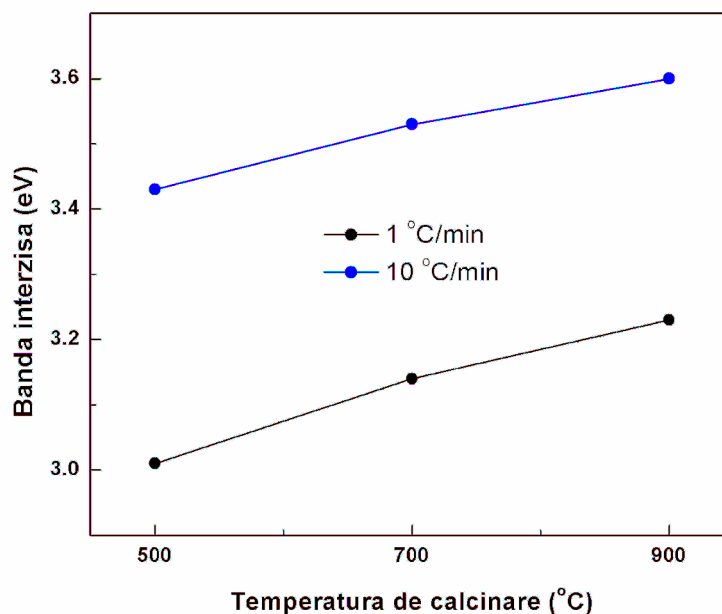
Figure 5.8. Variation of bandgap values as a function of temperature and heating rate of SnO_2 fibers calcination.

Chapter 6
Evaluation of corrosivity of foam concentrates used for fire extinguishing by long term immersion of metallic materials

6.1. Introduction
The corrosion of materials from the composition of the trucks for fire extinguishing using high efficacy foam was discussed. The corrosion problems when working with foam can occur on a wide range of complex devices, to which the storage and transport systems can be added.

6.2. Description of foam installation and working conditions
6.2.1. Installation for foam production
In all cases, the equipments for mechanical foam production serves to mix the concentrate with air and water and provides a concentration of 2 - 5 ‰ for the concentrate in the resulting foam. Due to the much improved extinguishing efficiency, the fire can be quenched more quickly, a larger fire field can be controlled and the damages caused by the foam, as well as the environmental pollution are limited.

The characteristics of the standard equipment in Romania, for the foam formation and spraying, are:
- water flow discharged through the generator - 1000 L/min;
- nominal consumption of liquid spumogen - 240 L/min;
- nominal foam flow using six generating pipes of type B - 30 m^3/min.

6.2.2. Characteristics of studied foam concentrates
The foam concentrates used in the experimental determinations are the assortments *6 % P Profoam 806* [153] and *Fomtec P 6 %* [154], which are currently used in Romanian fire extinguishing units. Both spumogens produce foam by mixing 6 volumetric parts concentrate with 94 volumetric parts water. The products *6 % P Profoam 806* and *Fomtec P 6 %* are designed to combat class B fires, of flammable liquids or solids. Both liquids are protein concentrates obtained from very carefully controlled mixtures of hydrolyzed proteins, foaming amplifiers, frost free additions, stabilizers and preservatives. They are dark brown, heavier than water, with higher viscosity than water and a freezing point below - 13 °C. The measured *p*H by was between 9 and 10, more alkaline than the one given by the companies. *6 % P* products are nontoxic and biodegradable.

Generally, the producing companies do not provide the chemical compositions of the foam concentrates, so the data for the two studied representative concentrates were difficult to collect.

6.2.3. Selection and preparation of metallic materials for corrosion testing in foam concentrates
Of the metallic materials involved in the foam preparation, *aluminium alloy*, material taken from the nozzles or Storz couplings for hoses, and *carbon steel*, from which the walls of spumogen tanks and the metalic pipes are made, were selected for the

experiments. The metallographic preparation of the samples was carried out according to the usual procedures: polishing, washing, drying and isolation with epoxy resin.

The own results for aluminium alloy samples show that the main alloying elements are silicon, copper, iron and magnesium, the material used for testing being similar to *AlSi5Cu1Mg* aluminium alloy [173].

Low carbon steel *OL 42.2* k is a commn steel for construction. The own experiments on the chemical composition of carbon steel show that the main alloying elements are carbon and manganese. On another hand, the inhomogeneity of steel mass is illustrated by the presence of insoluble inclusions containing metallic oxides, mainly aluminium and calcium oxides.

6.3. Gravimetric studies on aluminium alloy and carbon steel corrosion in foam concentrates

The gravimetric measurements of the corrosion rate were performed by immersion in each of the two spumogen concentrates for different periods of time, up to 348 days. The corrosion rate was estimated through the gravimetric index (k_g) and penetration index (*CR*). The preliminary tests for the profiled samples of aluminium alloy showed that this type of determination is very difficult to interpret because of the piece shape complexity, which leads to a difficult and unsafe removal of the corrosion products by simple washing.

Tables 6.15 and 6.16 include the values obtained for the two parameters. The k_g values for aluminium alloy are irrelevant and uncertain, in the sense that they are very different for identical samples after seven days of immersion, while after 14 days, only one of the samples presents weight loss. As a whole, the corrosion process may be considered to advance over time and, therefore, the gravimetric index and penetration index tend to grow, clearly indicating an instability of aluminium alloy in contact with the foam concentrate. Thus, it can be considered that the relatively high value of the penetration index (0.68 mm/year) demonstrates the aggressiveness of the concentrate on aluminium alloy parts from nozzles or Storz couplings.

Table 6.15. Corrosion integral (cumulative) gravimetric index (k_g)
for aluminium alloy, in *Foamtec P 6 %* foam concentrate.
The penetration index (*CR*) is given in brackets.

Aluminium alloy sample	$k_g \cdot 10^2$ *(g/m² h)* after different immersion periods of time In brackets: *CR (mm/year)*	
	7 days (168 h)	14 days (336 h)
1	0.54 (0.0175 mm/year)	21.07 (0.6836 mm/year)
2	0.10 (0.0324 mm/year)	33.04 (*weight increase)
3	0.77 (0.0245 mm/year)	29.09 (*weight increase)

The data obtained for carbon steel are reliable and reproducible. In the case of the samples immersed in *Foamtec P 6 %* concentrate, the corrosion intensifies especially during the end periods of immersion, while in *6 % P Profoam 806*, the corrosion has a relatively uniform rate. The corrosion rate significantly increases over time; this can be explained by the formation of complex compounds with proteins, that can catalyze the corrosion process. These compounds can remain or detach from the surface, so that the layer does not protect.

Table 6.16. Corrosion integral (cumulative) gravimetric
index (k_g) for carbon steel in the foam concentrates.
The penetration index (*CR*) is given in brackets.

Carbon steel sample	$k_g \cdot 10^2$ (g/m² h) after different immersion periods of time In brackets: *CR (mm/year)*				
	29 days (696 h)	63 days (1512 h)	81 days (1944 h)	232 days (5568 h)	348 days (8352 h)
Foamtec P 6 % concentrate					
1	1.063 (0.0118)	1.347 (0.0150)	1.366 (0.0152)	1.246 and 1.182* (0.0139) and (0.0132)	1.234 (0.0138)
2	1.106 (0.0123)	1.329 (0.0148)	1.335 (0.0149)	1.415 (0.0158)	1.530 (0.0171)
3	1.480 (0.0165)	1.774 (0.0198)	1.765 (0.0197)	2.320 (0.0258)	2.331 (0.0259)
6 % P Profoam 806 concentrate					
4	2.989 (0.0333)	4.001 (0.0446)	4.760 (0.0530)	3.622 and 3.011* (0.0404) and (0.0333)	4.252 (0.0474)
5	3.666 (0.0409)	5.831 (0.0650)	5.960 (0.0664)	4.664 and 3.968* (0.0520) and (0.0442)	5.075 (0.0566)
6	3.088 (0.0344)	4.121 (0.0459)	4.797 (0.0535)	3.793 and 3.254* (0.0423) and (0.0363)	4.411 (0.0492)

* The differential gravimetric index calculated for the period only between 81 and 232 days

6.4. Morphological and compositional characterization
6.4.1. Characterization of aluminium alloy surface after corrosion testing

The morphological analysis performed on the initial aluminium alloy samples illustrates the interdendritic arrangement of silicon in aluminium solid solution, as well as the existence of iron based insoluble compounds with acicular or polyhedral morphology.

A comparison between the morphology of the two aluminium alloy samples before (reference) and after (sample 1 and sample 2) the corrosion test by immersing for 348 h in *6 % P Profoam 806* concentrate is shown in Figure 6.8. It can be clearly observed the layer of corrosion products covering the metal surface and the fact that there are discontinuities (cracks), suggesting the lack of adhesion on the support material. From the anticorrosion protection point of view of, this is a drawback, meaning that the corrosion products do not protect.

From the comparison of the elemental compositions obtained on the surface of the initial aluminium alloy and on the surface exposed to the corrosive attack of the foam concentrate, changes were observed in the concentrations of all constitutive elements.
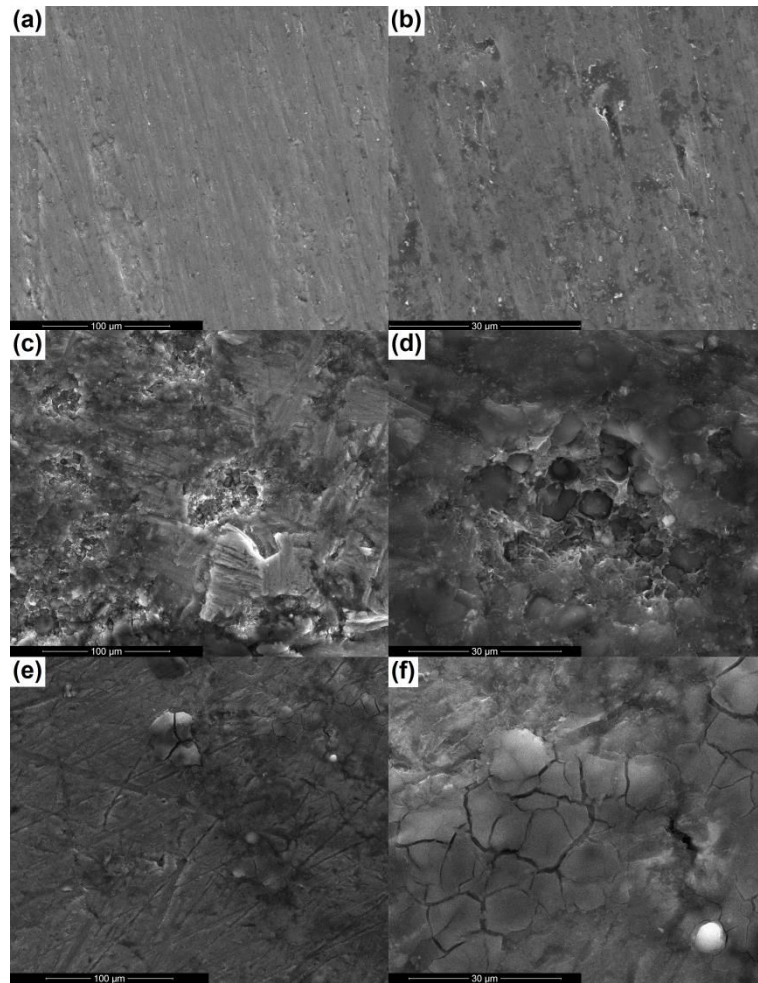
Figure 6.8. SEM images of aluminium alloy before and after immersion 348 h in *6 % P Profoam 806* concentrate: reference (a and b), sample 1 (c and d) and sample 2 (e and f).

6.4.2. Characterization of carbon steel surface after corrosion testing

The microstructure of carbon steel prior to the corrosion test has a relatively good homogeneity, except for an aggregate present in the analyzed area, which may be an intermetallic compound.

Carbon steel samples immersed in *Foamtec P 6 %* concentrate over a long period of time are covered with a noncompact film with numerous breaks of the coating, which represents areas for the continuous penetration of the aggressive liquid towards the metallic surface, followed by intense corrosion. Figure 6.14 shows how the destructive attack occurred within carbon steel mass, visible after the corrosion products removal; at higher magnifications, circular caverns and grooves in the sample mass are detected, all of which are the result of localized corrosion.

By comparing the corrosion products collected from the surface of the tested pieces with the initial composition of carbon steel, the way in which the alloying elements concentration changes can be seen, but also the appearance of nonmetallic elements specific to oxides/hydroxides or salts. Also, the corrosion products are not crystalline, the only phase identified based on the crystalline planes being NaCl.
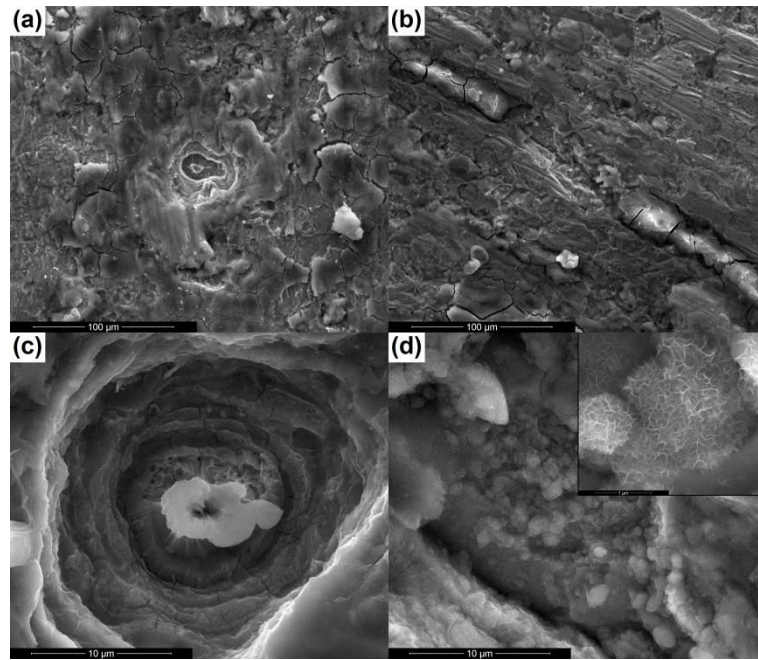
Figure 6.14. SEM images of carbon steel sample after immersion 166 days (3984 h) in *Foamtec P 6 %* concentrate and removal of the soluble corossion products by washing: overall aspect (a and b) and structures resulted after corossion (c and d).

Chapter 7
Electrochemical studies on aluminium alloy and carbon steel corrosion in foam concentrates

7.1. Cell, equipment and working methodology

The electrochemical cell was undivided and contained a volume of 100 - 150 mL electrolyte, unstirred, from *6 % P Profoam 806* or *Foamtec P 6 %* foam concentrates, as such or, in some determinations, half diluted solution with bidistilled water. The electrode to be investigated was either aluminium alloy in the form of profiled piece or carbon steel in the form of rectangular plate. In the electrochemical cell, the auxiliary electrode was a platinum plate and the reference electrode was Ag/AgCl/KCl.

The values of the corrosion potential E_{corr} and corrosion current density i_{corr} were experimentally determined using the potentiodynamic polarization curves (Tafel). The values of the polarization resistance Rp (parameter correlated with the corrosion rate) were determined by electrochemical impedance spectroscopy. [311,312]

7.2. Electrochemical studies for aluminium alloy
7.2.1. Potentiodynamic polarization curves

The Tafel curves for aluminium alloy in *Foamtec P 6 %* concentrate are shown in Figure 7.2. Table 7.1 lists the corrosion parameters values obtained by intersecting the Tafel slopes with the potential vertical at minimum current. The curve branch of the most negative potentials corresponds to the cathodic reduction of oxygen dissolved in NaCl nondeaerated solution. The right hand branch represents the anodic dissolution processes of aluminium alloy, with an active area starting from the corrosion potential, where the current suddenly increases, and then with a current limitation; this last part corresponds to a stationary state between the amount of corrosion products that detaches and falls into the solution and the new amount formed by material degradation. In the case of the half diluted solution, the aspect of Tafel curve is quasisimilar, but in addition current oscillations occur very clearly, both in the anodic and cathodic branches. These are characteristic of a more intense participation of water ions, but the corrosion parameters are not basically modified.
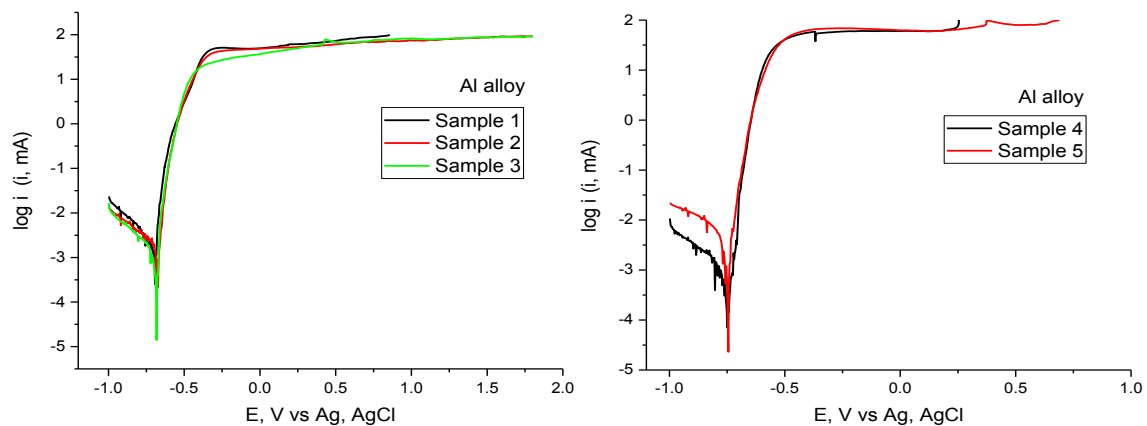
Figure7.2. Tafel curves for five samples (noted 1, 2, 3, 4 and 5) of aluminium alloy from nozzles or Storz couplings, in *Foamtec P 6 %* concentrate.

Table 7.1. Corrosion parameters values for
aluminium alloy, in *Foamtec P 6 %* concentrate.

Sample	E_{corr} vs. Ag/AgCl *(mV)*	log i_{corr}	$i_{corr} \cdot 10^3$ *(mA/cm²)*
Sample 1	- 695	- 2.840	1.445
Sample 2	- 677	- 2.715	1.927
Sample 3	- 677	- 2.890	1.288
Sample 4	- 747	- 3.100	0.794
Sample 5	- 740	- 2.560	2.750
Values range	between -670 and -740 mV	-	$1.64 \cdot 10^{-3}$ mA/cm²

Determinations in *6 % P Profoam 806* concentrate (Figure 7.10) were also made. Generally, the aspect of Tafel curve recorded for pure aluminium is similar to that of the curves obtained for aluminium alloy samples, with the exception that ample current oscillations clearly appear in the active area (potentials between - 0.6 and - 0.5 V). In addition, a difference of about 100 mV with respect to E_{corr} was identified for pure aluminium, being more negative than the potentials resulted for aluminium alloy. E_{corr} values between - 680 and - 780 mV and i_{corr} values between 3 and 10 µA/cm² (average 2 µA/cm²) resulted from the experimental data for ten aluminium alloy samples.
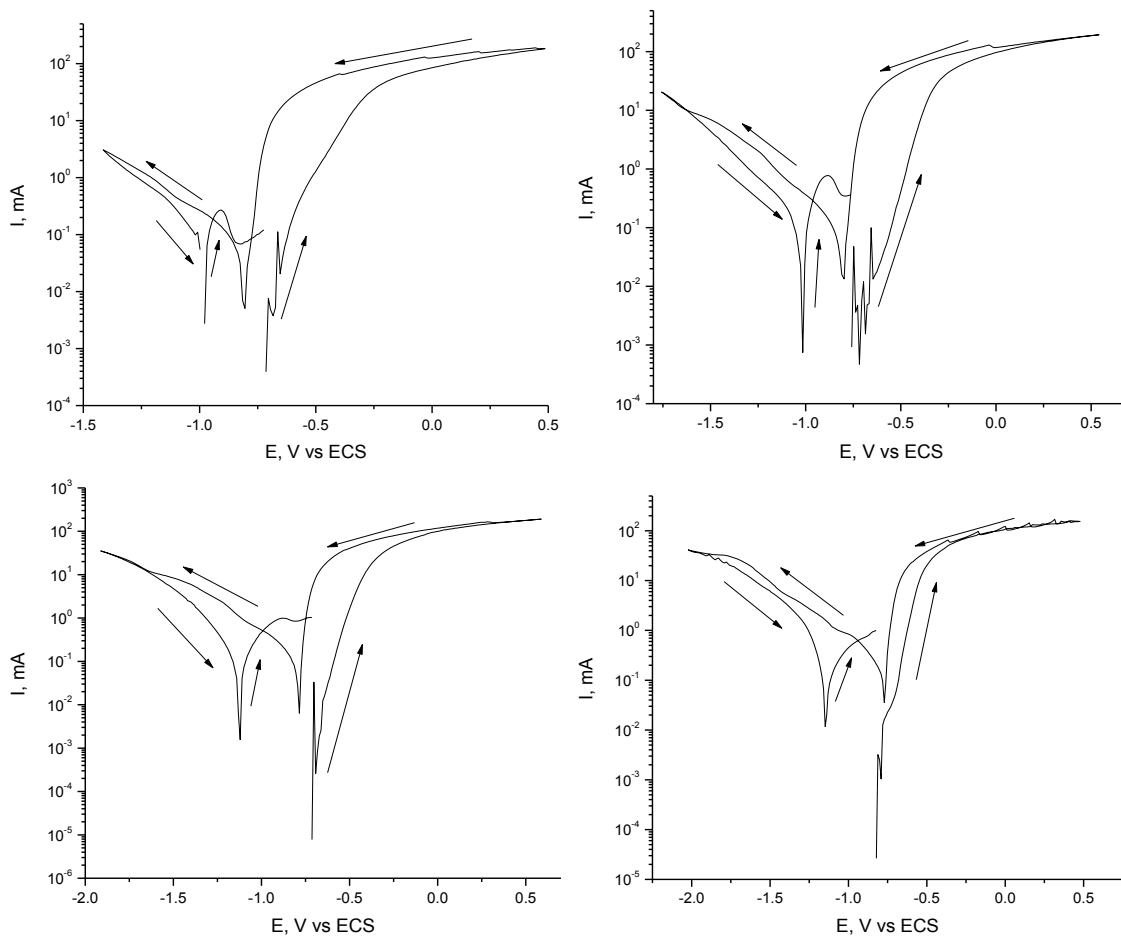
Figure 7.10. Tafel curves for four samples (noted 1, 2, 3 and 4) of
aluminium alloy from Storz couplings, in *6 % P Profoam 806* concentrate.

7.2.2. Electrochemical impedance spectra

From the EIS spectra obtained for aluminium alloy samples (Figure 7.13) it is observed that all Nyquist semicircles have a snail like shape, characteristic of the corrosion with the formation of insoluble products, which adsorb on the surface of the electrode. Their diameters have values that gradually decrease with the anodic polarization, confirming the increasingly intense material corrosion. At polarization very close to the stationary potential, the R_p value is about 25000 $\Omega \cdot cm^2$ for *6 % P Profoam 806* concentrate, but for *Foamtec P 6 %* barely exceeds 150 $\Omega \cdot cm^2$; this means that in the second environment, the corrosion process has a much faster rate and a shortening of the induction range for the active corrosion zone is recorded. Consequently, the impedance modulus in the Bode diagrams decreases with anodic polarization increasing. It is to be noted that all values for the Bode phase angle are negative, confirming that in the corrosion processes the interfaces act only as resistors and capacitors, without inductances. It is also proven that *Foamtec P 6 %* is more aggressive than *6 % P Profoam 806*.

(a)

(b)

(c)
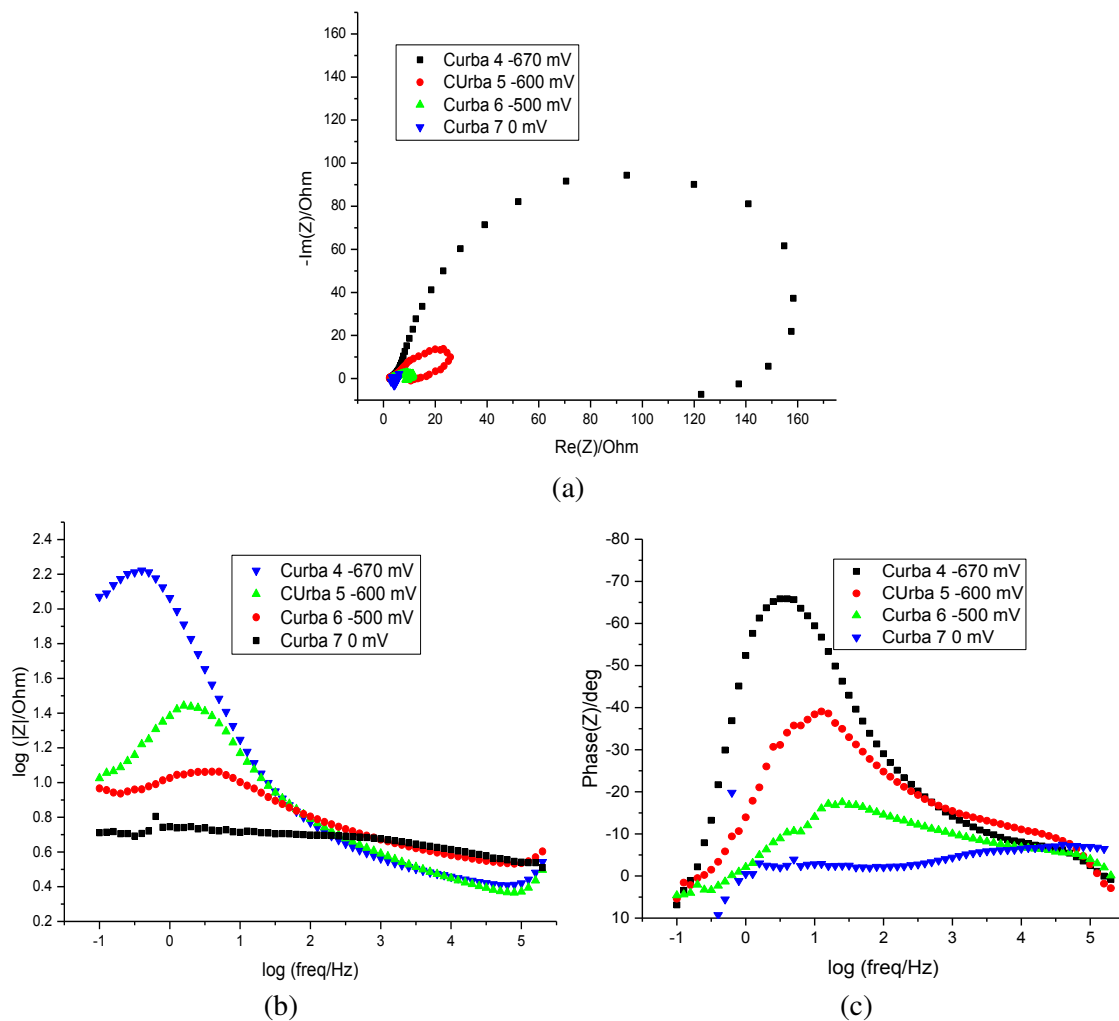
Figure 7.13. Nyquist spectra (a), Bode - impedance modulus (b) and Bode - phase angle (c) for aluminium alloy, in *Foamtec P 6 %* concentrate, at different polarization potentials.

A validation of data was achieved by modeling with a Randles equivalent electric circuit, where *Rs* represents the solution ohmic resistance, *R1* is the charge transfer resistance, which in corrosion is called polarization resistance *Rp*, and *CPE1* symbolizes

the capacitance of the electrochemical double layer. The constant phase element has *CPE1-T* (capacitive part) and *CPE1-p* (exponent) components.

Table 7.3 gives the circuit parameter values for the best fitting. It is observed that constant values of *Rs* (3 - 4 $\Omega \cdot cm^2$) and also plausible values of *CPE1* (11 - 125 $\mu F/cm^2$), which ideally in aqueous solutions is 30 - 100 $\mu F/cm^2$, were obtained. The *CPE-p* values (0.92 - 1.00) confirm the good modeling quality and the near ideal behavior of *CPE1*. In the final column, the *Rp* values decrease continuously, demonstrating the continuous corrosion of aluminium alloy.

Table 7.3. Equivalent circuit parameters values resulted from the best fitting of the experimental data for aluminium alloy, in *6 % P Profoam 806* concentrate.

Polarization potential	Rs ($\Omega \cdot cm^2$)	CPE1-T$\cdot 10^5$ ($\mu F/cm^2$)	CPE1-p	Rp ($\Omega \cdot cm^2$)
- 705 mV	3.30	11.198	0.939	5352.0
- 690 mV	3.20	9.701	0.948	3933.0
- 705 mV	4.40	2.860	0.926	22316.0
- 477 mV	2.50	9.939	0.938	21.0
- 611 mV	2.60	12.547	0.926	78.0
- 483 mV	4.10	1.095	1.010	16.0
- 295 mV	4.20	1.358	1.018	7.4
- 84 mV	4.20	1.306	1.016	3.5
+ 115 mV	4.24	2.450	0.920	3.4

7.3. Electrochemical studies for carbon steel
7.3.1. Potentiodynamic polarization curves

Figures 7.24 and 7.26 show the Tafel curves for carbon steel samples immersed in the two foam concentrates. Overall, the i_{corr} values are comparable to those for the aluminium alloy, but the E_{corr} values are more positive with about 100 mV. It turns out that low alloy carbon steel is a metallic material nobler than aluminium alloy.

(a)   (b)

(c)
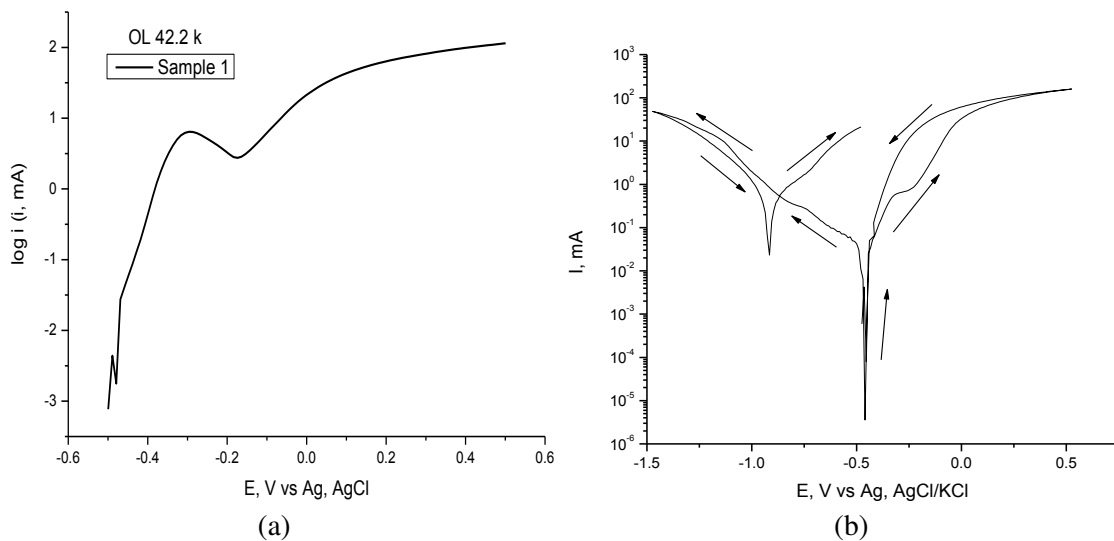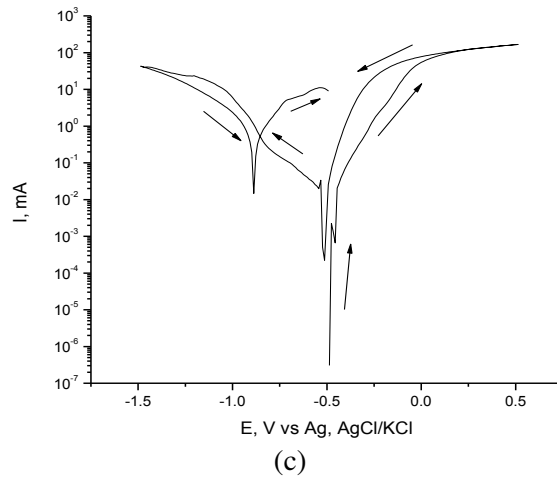
Figure 7.24. Tafel curves for three identical samples of carbon steel, in *6 % P Profoam 806* concentrate. The scanning starts anodically.

(a)   (b)
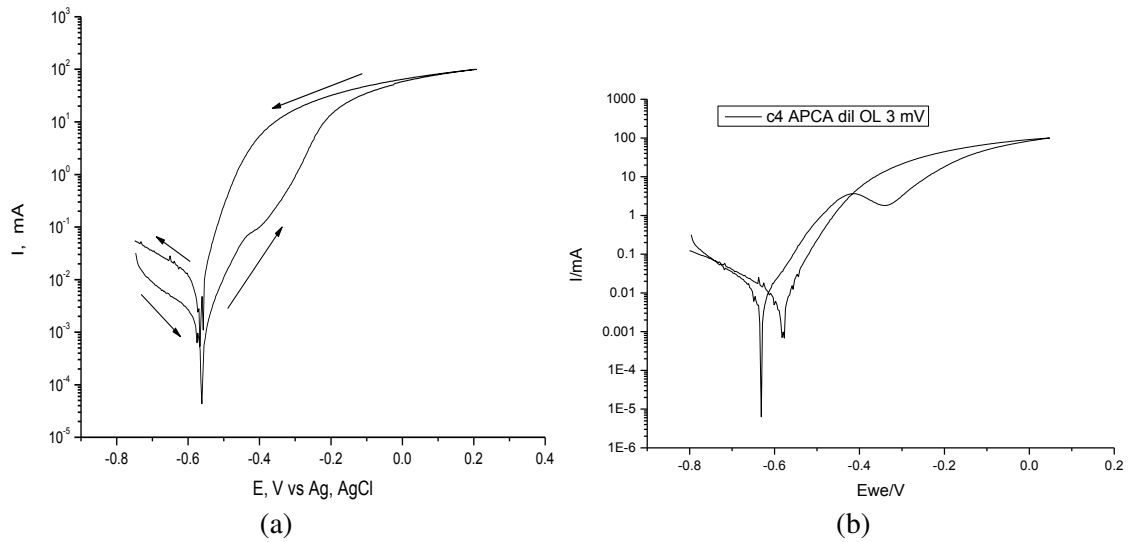
Figure 7.26. Tafel curves for two identical samples of carbon steel, in *Foamtec P 6 %* concentrate: undiluted concentrate (a) and half diluted concentrate (b).

7.3.2. Electrochemical impedance spectra

From the EIS spectra obtained for carbon steel samples (Figure 7.27) it is obvious that the Nyquist semicircles have a linear part at their end, which can be attributed to the formation of an insoluble film on the electrode surface; the horizontal position indicates an unstable film, possibly with products that detach or are soluble in the liquid. Then, at high anodic polarizations, the semicircles have a snail like shape, twisted inwards, meaning that the formed products are less adsorbed. However, the main characteristic of the semicircles is the diameter reduction at low anode overpotentials (up to - 835 mV), indicating the corrosion enhancement, and from - 825 to - 435 mV, the increase in diameter, suggesting a more stable passivation. Bode phase angle diagrams indicate a surface semiconductor behavior of the surface.
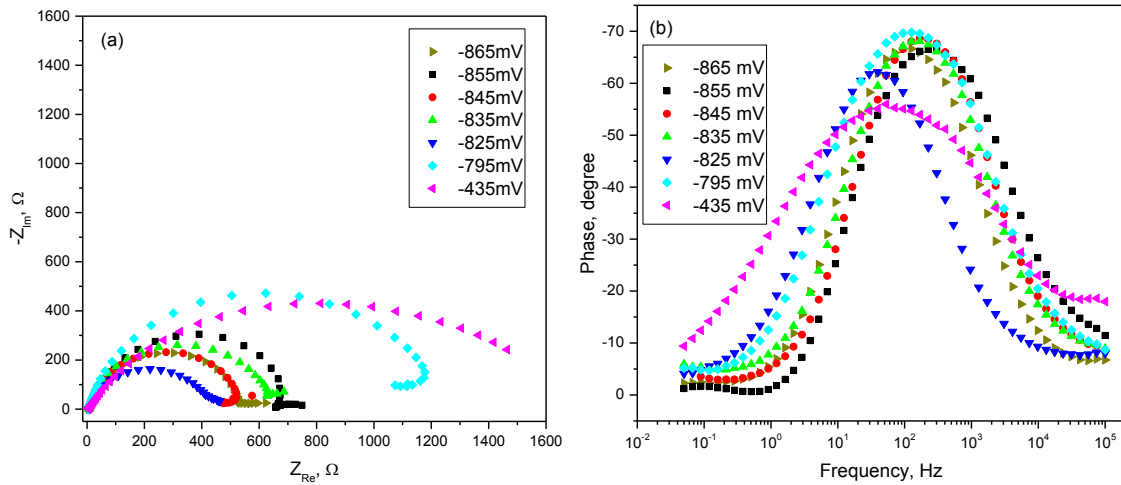
Figure 7.27. Nyquist spectra (a) and Bode - phase angle (b) for carbon steel,
in *6 % P Profoam 806* concentrate, at different polarization potentials.

Table 7.4 displays the circuit parameters values after data modeling. The safest results are for *Rs*, where most values are relatively close (in the range 6 - 7 $\Omega \cdot$cm^2). *CPE1* values (23 - 170 μF/cm^2) in *6 % P Profoam 806* concentrate are in the normal range for aqueous solutions. The electrode/electrolyte interface behaves less ideally than in the case of aluminium alloy, but the *CPE1-p* exponent is still in the acceptable area (0.7 - 0.9). A more unusual result is the evolution of the *Rp* values, which has fluctuations and does not show a firm decreasing trend, to indicate the growth of i_{corr}.

Table 7.4. Equivalent circuit parameters values resulted from the best fitting of
the experimental data for carbon steel, in *6 % P Profoam 806* concentrate.

Polarization potential	Rs ($\Omega \cdot$cm^2)	CPE1-T$\cdot$10^5 (μF/cm^2)	CPE1-p	Rp ($\Omega \cdot$cm^2)
- 865mV	7.2	4.8539	0.875	558.4
- 855 mV	6.8	2.3334	0.862	699.2
- 845 mV	6.4	2.9873	0.890	525.7
- 835 mV	6.4	12.6490	0.746	1128.0
- 825 mV	7.7	17.7330	0.825	439.3
- 795 mV	5.9	4.1285	0.852	1180.0
- 435 mV	5.1	22.4440	0.664	1572.0

CONCLUSIONS

General conclusions

SnO_2 powders were successfully prepared by four wet chemistry methods: precipitation, sol-gel, Pechini and hydrothermal. SnO_2 powders doped with La^{3+} or V^{5+} were synthesized by the precipitation method, followed by a calcination step. Such zerodimensional structures can be easily integrated into nanoscale devices for the field of gas sensors.

SnO_2 based ceramics, doped with La^{3+} or V^{5+}, were obtained by sintering the precipitation derived powders. In general, a doping proportion of 0.5 - 1.0 wt% and a thermal treatment at lower temperatures are indicated, so as to obtain characteristics suitable for the sensors field. Lanthanum improves the behavior of SnO_2 based ceramics in the presence of isopropyl alcohol vapors, while vanadium has a beneficial effect in the case of methane atmosphere.

SnO_2 fibers were successfully synthesized by electrospinning, followed by calcination. The bandgap values falls within the range 3.0-3.6 eV, which highlights the possibility of adjusting the optical properties to a large extent without the use of additives or dopants. SnO_2 fibers suitable for gas sensor applications can be obtained in the case of a small calcination temperature and a low heating rate.

The corrosivity of *6 % P Profoam 806* and *Foamtec P 6 %* foam concentrates used for fire extinguishing was studied, regarding the degradation of aluminium alloy from which various components are made (Storz couplings for hose reels and nozzles for foam spraying), as well as the degradation of carbon steel walls of the tanks in which the foam concentrate is stored and of its transport pipes.

Firstly, gravimetric determinations of corrosion rate at long term immersion of metallic materials, expressed as gravimetric index and penetration index, were made. The obtained values for aluminium alloy are irrelevant and uncertain, while for carbon steel, they are reliable and reproducible. The morphological and compositional characterization of the studied materials surface was performed before and after the corrosion process, highlighting the effects of the corrosive attack: the appearance of corrosion products, the formation of pits/caverns or cracks/grooves, as well as changes in the concentrations of all constitutive elements. The corrosion reactions are strongly influenced by the microstructure and composition of the materials in contact with the foam concentrate.

Two electrochemical methods were also approached: Tafel polarization curves and electrochemical impedance spectroscopy. The application of the first method made possible the corrosion potential and corrosion current density determination by cyclic polarization, under potentiodynamic conditions. Valuable information was extracted from the electrochemical impedance spectra at open circuit potential and a number of increasingly positive potentials that simulate the advancement of metal anodic dissolution. The experimental data modeling was performed with a Randles equivalent electrical circuit. It was shown that low alloy carbon steel is a metallic material nobler than aluminium alloy. On another hand, *Foamtec P 6 %* is more aggressive than *6 % P Profoam 806*.

Original contributions

The originality of the doctoral thesis can be summarized in the following ideas:

● investigating the influence of the wet chemistry synthesis method on the structural and morphological properties of SnO_2 zerodimensional structures;

● approaching doping species (La^{3+} and V^{5+}) little studied for SnO_2 structures;

● studying the influence of dopant nature and amount on the optical properties of SnO_2 powders;

● selecting new processing conditions for SnO_2 ceramics;

● investigating the effect of dopant type and concentration and sintering temperature on the response of SnO_2 based ceramics in the presence of methane or isopropyl alcohol vapors;

● correlating the performance of SnO_2 based gas sensors with the composition, crystal structure, size, shape and surface of the active material;

● controlling the bandgap energy values of electrospun SnO_2 fibers by means of synthesis conditions;

● studying for the first time the corrosivity of *6 % P Profoam 806* and *Foamtec P 6 %* foam concentrates on two metallic materials used in the construction of equipments employed by firefighters;

● characterizing the aluminium alloy and carbon steel from morphological and compositional point of view in order to report to standards;

● estimating of corrosion rate, expressed as gravimetric index and penetration index, by weighing the samples before and after immersion in foam concentrates;

● determining the corrosion potential and corrosion current density by cyclic polarization, under potentiodynamic conditions, for all spumogen - metallic material combinations;

● characterizing the corrosion products from structural, morphological and compositional point of view, as well as highlighting the investigated materials degradation after the aggressive attack;

● applying the electrochemical impedance spectroscopy to highlight the corrosion process characteristics for aluminium alloy and carbon steel in *6% P Profoam 806* and *Foamtec P 6%* foam concentrates;

● modeling the experimental data with a Randles equivalent electrical circuit and extracting the values for the solution resistance, double layer capacity and polarization resistance.

SELECTIVE BIBLIOGRAPHY

[4] *X. Liu, S. Cheng, H. Liu, S. Hu, D. Zhang, H. Ning*, A survey on gas sensing technology, Sensors 12 (2012) 9635-9665.

[8] www.msasafety.com, 02.11.2017.

[9] *C. Wang, L. Yin, L. Zhang, D. Xiang, R. Gao*, Metal oxide gas sensors: Sensitivity and influencing factors, Sensors 10 (2010) 2088-106.

[11] www.ehstoday.com, 02.11.2017.

[12] www.figaro.co.jp, 03.11.2017.

[16] *M.E. Franke, T.J. Koplin, U. Simon*, Metal and metal oxide nanoparticles in chemiresistors: Does the nanoscale matter?, Small 2 (2006) 36-50.

[17] *R.D. Delgado*, Tin oxide gas sensors: An electrochemical approach, PhD Thesis, University of Barcelona, 2002.

[26] *J. Robertson, B. Falabretti*, Electronic structure of transparent conducting oxides (Chapter 2), Handbook of transparent conductors (Editor *D.S. Ginley*), Springer Science + Business Media LLC, 2010.

[29] *M. Batzill, U. Diebold*, The surface and materials science of tin oxide, Progress in Surface Science, 79 (2005) 47-154.

[31] *D. Neamen*, Semiconductor physics and devices, McGraw-Hill, New York, 2003.

[36] *J.G. Kang, J.S. Park, H.J. Lee*, Pt-doped SnO_2 thin film based micro gas sensors with high selectivity to toluene and HCHO, Sensors and Actuators B 248 (2017) 1011-1016.

[60] *Z. Jiang, R. Zhao, B. Sun, G. Nie, H. Ji, J. Lei, C. Wang*, Highly sensitive acetone sensor based on Eu-doped SnO_2 electrospun nanofibers, Ceramics International 42 (2016) 15881-15888.

[75] *B. Babu, A.N. Kadam, R.V.S.S.N. Ravikumar, C. Byon*, Enhanced visible light photocatalytic activity of Cu-doped SnO_2 quantum dots by solution combustion synthesis, Journal of Alloys and Compounds 703 (2017) 330-336.

[78] *L. Cheng, S.Y. Ma, T.T. Wang, X.B. Li, J. Luo, W.Q. Li, Y.Z. Mao, D.J. Gz*, Synthesis and characterization of SnO_2 hollow nanofibers by electrospinning for ethanol sensing properties, Materials Letters 131 (2014) 23-26.

[120] www.nrl.navy.mil, 09.11.2017.

[123] Regulation (EC) No 648/2004 of the European Parliament and of the Council of 31 Match 2004 on Detergents.

[124] Co-operation on existing chemicals: Hazard assessment of perfluorooctane sulfonate (PFOS) and its salt, Environment Directorate: Joint Meeting of the Chemicals Committee and the Working Party on Chemicals, Pesticides and Biotechnology, 2002, 5.

[125] *B. Krol, K. Prochaska, L. Chrzanowski*, Biodegradability of firefighting foams, Fire Technology 48 (2012) 173-181.

[126] *A. Bourgeois, J. Bergendahl, A. Rangwala*, Biodegradability of fluorinated fire-fighting foams in water, Chemosphere 131 (2015) 104-109.

[127] *C. Fang, M. Megharaj, R. Naidu*, Surface-enhanced Raman scattering (SERS) detection of fluorosurfactants in firefighting foams, RSC Advances 6 (2016) 11140-11145.

[147] www.chemguard.com, 11.11.2017.

[148] www.solbergfoam.com, 11.11.2017.

[149] www.linkedin.com, Luoyang Langchao Fire Technology, 11.11.2017.

[150] www.ansul.com, 11.11.2017.

[151] www.angusfire.com, 11.11.2017.

[152] www.chemours.com şi www.dupont.com, 11.11.2017.

[153] www.profoam.it, 11.11.2017.

[154] www.fomtec.com, 11.11.2017.

[168] *C. Babut, N. Ungureanu, M. Ungureanu*, Research on fire hose couplings damages, IOP Conference Series: Materials Science and Engineering, 163 (2017) 012016.

[170] *P. Su, D.B. Fuller*, Corrosion and corrosion mitigation in fire protection systems, Research Technical Report, 0003040794, FM Global, Norwood, 2014.

[172] *H. Goto, M. Ashida, K. Endo*, The influence of oxygen and water vapour on the friction and wear of an aluminum alloy under fretting conditions, Wear 116 (1987) 141-155.

[173] *M. Wierzbinska, J. Sieniawski*, Effect of morphology of eutectic silicon crystals on mechanical properties and cleavage fracture toughness of AlSi5Cu1 alloy, Journal of Achievements in Materials and Manufacturing Engineering 14 (2006) 31-36.

[174] BS EN 1706:2010, Aluminium and aluminium alloys. Castings. Chemical composition and mechanical properties.

[175] *M.I. Niţu*, Cercetări privind îmbunătăţirea unor proprietăţi fizico-mecanice la aliajele de aluminiu turnabile prin intermediul tratamentelor termice, Teză de Doctorat, Universitatea Transilvania din Braşov, 2010.

[176] *Z. Rajic, M. Torkar, I. Paulin, B. Zuzek, C. Donik, M. Bizjak*, Properties of AlSi5Cu1Mg modified with Sb, Sr and Na, Materials and Technology 48 (2014) 991-996.

[177] *B. Li, X. Tang, Y. Zuo*, Experimental research on mechanical properties of 5083 aluminum alloy for fitness-for-service assessment of cryogenic pressure vessel after fire exposure, AIP Conference Proceedings 1829 (2017) 020022.

[178] *W.B. Jamison, N. Rainaldi, W.W. Harpur*, Advancements in extinguishants. A symposium, Fire Journal 63 (1969) 32-43.

[181] *P. Su, F.W. Tatar, S. Chivukula, W.W. Doerr*, Weld seam corrosion of steel sprinkler pipe, NACE International, NACE-2013-2140, Orlando, 2013.

[183] Corrosion in automatic sprinkler systems, FM Global, Property Loss Prevention Data Sheets, 2016.

[188] *T. Sasaki, Y. Miyazato, J. Inamoto, T. Yamamoto, A. Nakamura*, Development of firefighting equipment for efficient firefighting strategy (Development of new nozzle), Journal of Disaster Research 10 (2015) 620-625.

[202] *C. Jinga, D. Berger, C. Matei, S. Jinga, E. Andronescu*, Characterization of $BaMg_{1/3}(Ta_{1-x}Nb_x)_{2/3}O_3$ ceramics obtained by a modified Pechini method, Journal of Alloys and Compounds 497 (2010) 239-243.

[203] *G. Voicu, V.L. Ene, D.F. Sava, V.A. Surdu, C. Busuioc*, Sol-gel derived vitroceramic materials for biomedical applications, Journal of Non-Crystalline Solids 449 (2016) 75-82.

[205] *C. Busuioc, A. Evanghelidis, M. Enculescu, I. Enculescu*, Optical and photocatalytic properties of electrospun ZnO fibers, Digest Journal of Nanomaterials and Biostructures 10 (2015) 957-965.

[211] *K. Rubenis, S. Populoh, P. Thiel, S. Yoon, U. Muller, J. Locs*, Thermoelectric properties of dense Sb-doped SnO_2 ceramics, Journal of Alloys and Compounds 692 (2017) 515-521.

[212] *T.I. Gandhi, R.R. Babu, K. Ramamurthi, M. Arivanandhan*, Effect of Mn doping on the electrical and optical properties of SnO_2 thin films deposited by chemical spray pyrolysis technique, Thin Solid Films 598 (2016) 195-203.

[213] *L.A. Ma, Z.H. Wei, X.Y. Ye, T. Lin, T.L. Guo*, Structure and enhanced field emission properties of cone-shaped Zn-doped SnO_2 nanorod arrays on copper foil, Materials Letters 174 (2016) 32-35.

[214] *X. Lian, Y. Li, X. Tong, Y. Zou, X. Liu, D. An, Q. Wang*, Synthesis of Ce-doped SnO_2 nanoparticles and their acetone gas sensing properties, Applied Surface Science 407 (2017) 447-455.

[215] *P. Dou, Z. Cao, C. Wang, J. Zheng, X. Xu*, Multilayer Zn-doped SnO_2 hollow nanospheres encapsulated in covalently interconnected three-dimensional graphene foams for high performance lithium-ion batteries, Chemical Engineering Journal 320 (2017) 405-415.

[216] *C. Busuioc, S.I. Jinga*, Characterization of $LiZnVO_4$ ceramics prepared by two different methods, Journal of Optoelectronics and Advanced Materials 15 (2013) 1470-1474.

[217] *V. Bilovol, C. Herme, S. Jacobo, A.F. Cabrera*, Study of magnetic behaviour of Fe-doped SnO_2 powders prepared by chemical method, Materials Chemistry and Physics 135 (2012) 334-339.

[218] *S. Nilavazhagan, S. Muthukumaran, M. Ashokkumar*, Structural, optical and morphological properties of La, Cu co-doped SnO_2 nanocrystals by co-precipitation method, Optical Materials 37 (2014) 425-432.

[219] *X. Zhong, B. Yang, X. Zhang, J. Jia, G. Yi*, Effect of calcining temperature and time on the characteristics of Sb-doped SnO_2 nanoparticles synthesized by the sol-gel method, Particuology 10 (2012) 365-370.

[220] *P.V. Tuan, L.T. Hieu, L.Q. Nga, N.D. Dung, N.N. Ha, T.N. Khiem*, Hydrothermal synthesis and characteristic photoluminescence of Er-doped SnO_2 nanoparticles, Physica B 501 (2016) 34-37.

[221] *Y.H. Cho, X. Liang. Y.C. Kang, J.H. Lee*, Ultrasensitive detection of trimethylamine using Rh-doped SnO_2 hollow spheres prepared by ultrasonic spray pyrolysis, Sensors and Actuators B 20 (2015) 330-337.

[224] ***A.D. Busuioc***, *T. Vişan*, SnO_2 powders obtained by wet chemistry methods, 20th Romanian International Conference on Chemistry and Chemical Engineering (RICCCE 20), Septembrie 2017, Poiana Braşov, România.

[225] ***A.D. Busuioc***, *T. Vişan*, SnO_2 powders prepared by wet chemistry methods, University POLITEHNICA of Bucharest Scientific Bulletin B 79 [4] (2017) 33-40.

[226] ***A.D. Busuioc***, *R. Enuţă, Ş. Stoleriu, O. Oprea, T. Vişan*, SnO_2 powders doped with La^{3+} or V^{5+}, Romanian Journal of Materials 47 [3] (2017) 293-297.

[227] *S. Kitabayashi, N. Koga*, Thermal decomposition of tin(II) oxyhydroxide and subsequent oxidation in air: Kinetic deconvolution of overlapping heterogeneous processes, The Journal of Physical Chemistry C 119 (2015) 16188-19199.

[245] *T.A. Miller, S.D. Bakrania, C. Perez, M.S. Wooldridge*, Nanostructured tin dioxide materials for gas sensor applications (Chapter 30), Functional nanomaterials (Editors *K.E. Geckeler, E. Rosenberg*), American Scientific Publishers, 2006.

[246] *R. Vargas-Bernal, G Herrera-Perez*, Importance of the nanostructured ceramic materials on gas sensing (Chapter 1), Nanotechnology for optics and sensors (Editor *M. Aliofkhazraei*), One Central Press, 2014.

[248] *G. Korotcenkov*, Handbook of gas sensor materials: Properties, advantages, and shortcomings for applications, Volume 1: Conventional approaches, Springer, 2013.

[249] *G. Korotcenkov*, Handbook of gas sensor materials: Properties, advantages, and shortcomings for applications, Volume 2: New trends and technologies, Springer, 2014.

[255] ***A.D. Busuioc***, *R. Enuţă, Ş. Stoleriu, T. Vişan*, SnO_2 based ceramics for gas sensors, Romanian Journal of Materials 47 [4] (2017) 419-424.

[262] *J. Zhu, G. Zhang, S. Gu, B. Lu*, SnO_2 nanorods on ZnO nanofibers: A new class of hierarchical nanostructures enabled by electrospinning as anode material for high-performance lithium-ion batteries, Electrochimica Acta 150 (2014) 308-313.

[263] *X.X. Fan, X.L. He, J.P. Li, X.G. Gao, J. Jia*, Ethanol sensing properties of hierarchical SnO_2 fibers fabricated with electrospun polyvinylpyrrolidone template, Vacuum 128 (2016) 112-117.

[264] *E. Nikan, A.A. Khodadadi, Y. Mortazavi*, Highly enhanced response and selectivity of electrospun ZnO-doped SnO_2 sensors to ethanol and CO in presence of CH_4, Sensors and Actuato B 184 (2013) 196-204.

[265] *Z. Huang, H. Gao, Q. Wang, Y. Zhao, G. Li*, Fabrication of amorphous $SnO_2@C$ nanofibers as anode for lithium-ion batteries, Materials Letters 186 (2017) 231-234.

[267] *X. Kou, C. Wang, M. Ding, C. Feng, X. Li, J. Ma, H. Zhang, Y. Sun, G. Lu*, Synthesis of Co-doped SnO_2 nanofibers and their enhanced gas-sensing properties, Sensors and Actuators B 236 (2016) 425-432.

[268] *S. Liu, B. Yu, F. Li, Y. Ji, T. Zhang*, Coaxial electrospinning route to prepare Au-loading SnO_2 hollow microtubes for non-enzymatic detection of H_2O_2, Electrochimica Acta 141 (2014) 161-166.

[269] *Y. Zhao, X. He, J. Li, X. Gao, J. Jia*, Porous CuO/SnO$_2$ composite nanofibers fabricated by elec and their H$_2$S sensing properties, Sensors and Actuators B 165 (2012) 82-87.

[271] *S.W. Choi, A. Katoch, G.J. Sun, S.S. Kim*, Synthesis and gas sensing performance of ZnO-SnO$_2$ nanofiber-nanowire stem-branch heterostructure, Sensors and Actuators B 181 (2013) 787-794.

[272] *S.H. Yan, S.Y. Ma, X.L. Xu, W.Q. Li, J. Luo, W.X. Jin, T.T. Wang, X.H. Jiang, Y. Lu, H.S. Song*, Preparation of SnO$_2$-ZnO hetero-nanofibers and their application in acetone sensing performance, Materials Letters 159 (2015) 447-450.

[278] *B.R. Koo, S.T. Oh, H.J. Ahn*, Camphene effect for morphological change of electrospun SnO$_2$ nanofibers: From dense to fiber-in-hollow and to hollow nanostructures, Materials Letters 178 (2016) 288-291.

[279] *A. Macagnano, E. Zampetti, E. Kny*, Electrospinning for high performance sensors, Springer, 2015.

[280] *A.B. Suryamas, G.M. Anilkumar, S. Sago, T. Ogi, K. Okuyama*, Electrospun Pt/SnO$_2$ nanofibers as an excellent electrocatalysts for hydrogen oxidation reaction with ORR-blocking characteristic, Catalysis Communications 33 (2013) 11-14.

[281] *A. Katoch, J.H. Byun, S.W. Choi, S.S. Kim*, One-pot synthesis of Au-loaded SnO$_2$ nanofibers and their gas sensing properties, Sensors and Actuators B 202 (2014) 38-45.

[282] ***A.D. Busuioc****, I. Ciovică, Ş. Stoleriu, M. Enculescu, A. Evanghelidis, T. Vişan*, Morphological and optical properties of electrospun SnO$_2$ fibers, Digest Journal of Nanomaterials and Biostructures 12 [4] (2017) 1097-1105.

[311] ***A.D. Busuioc****, A. Cojocaru, A. Cotârţă, T. Vişan*, Corrosion of some steels and aluminium alloys in the foam concentrate used as fire-extinguishing medium, 16th International Conference of Physical Chemistry, (ROMPHYSCHEM 16 - 2016), Septembrie 2016, Galaţi, România.

[312] ***A.D. Busuioc****, A. Cojocaru, A. Cotârţă, T. Vişan*, Corrosion of an aluminium alloy and carbon steel in the foam concentrate used as fire-extinguishing medium, Manuscris ce va trimis spre publicare la revista Fire Technology.